Introduction to Charm Decay Analysis in Fixed Target Experiments

Ignacio Bediaga and Carla Göbel

Centro Brasileiro de Pesquisas Físicas,
Rio de Janeiro, Brazil

Abstract

We present an introduction to data analysis in Experimental High Energy Physics, and some concepts and useful tools are discussed. To illustrate, we use the data of E-791, a fixed target experiment recently realized at Fermilab. In particular, we analyse decay modes of D^+ meson with three charged particles in the final state.

Key-words: Experimental High Energy Physics, Charm Decays, Data Analysis

Course presented in the *V Taller Latino-Americano de Fenomenología de las Interacciones Fundamentales*, held on Puebla-Mexico in october/november 1995. To be published in the proceedings of this conference by the American Institute of Physics (AIP), New York.

CBPF-MO-001/96

Introduction

After 21 years of experimental research on charm particles, most of their characteristics like quantum numbers, lifetimes, dominant decay modes, excited states and production mechanisms are well established. For charm mesons, even rare decay modes like Doubly Cabibbo Supressed decays have been observed. For charm baryons, however, there is less information. For example, for the most studied charm baryon, Λ_c, the sum of all observed partial decay widths is less than half of the total width. Thus, many of its decay modes are still not observed.

But why there is particular interest in the study of charm particles? The most general answer to this question cannot be different from the answer of why we study elementary particles: the study of the elementary particles is the study of the fundamental interactions of nature.

Based on this context, the study of charm particles is particularly privileged. Their masses, around 2 GeV, allow a treatement based on assymptotic freedom, as for B mesons; on the other hand, there are still non-pertubative effects, as for strange mesons. As we know, non-pertubative effects represent one of the greatest difficulties of QCD in the study of strong interactions. One possible way to deal with these difficulties is to use charm mesons as a "laboratory", based precisely on their "semi-pertubative" features: simplicity of the pertubative treatement and at the same time the presence of some non-pertubative effects.

As an illustration of this fact, let's observe the differencies of the lifetimes for mesons of the same family:

$$\begin{aligned} \tau(K^+) &\sim 640\ \tau(K_s) & mass(K's) &\sim 0.5GeV \\ \tau(D^+) &\sim 2.5\ \tau(D^0) & mass(D's) &\sim 2GeV \\ \tau(B^+) &\sim \tau(B^0) & mass(B's) &\sim 5GeV\ . \end{aligned} \tag{1}$$

The energy range that distinguishes between the distinct meson families varies from the non-pertubative region (strange meson masses) to the pertubative region (B meson masses). One very possible explanation for the difference on the lifetimes is due to non-pertubative effects. In equation (1) we can have an idea of the influence of these effects comparing the difference of the mean lifetimes and masses for each family. As we said before, charm mesons are in a range of transition between non-pertubative and pertubative regions.

There are two other important features in the study of charm particles as "laboratory" for the interactions: a high diversity of decay modes and also a small multiplicity for these channels. In fact, an expressive part of hadronic decays has two bodies at the final state. The first feature allows a variety of possible channels to be studied and the second allows experimentally these studies, since it is easier to observe decays with a few particles in the final state.

The semi-pertubative features and the high diversity of channels with low multiplicity allow, for example, theoretical studies of non-leptonic decays.

Due to the semi-pertubative nature, it is possible to use factorization for a "current-current" matrix element, based on Valence Quark Approximation (VQA) model [1], while a two body decay can be parametrized with known matrix elements. With over than 50 observed two-body decay channels for the D^+, D^0 and D_s^+ pseudo-scalar mesons, any theoretical model has, with this experimental information, a good place to test the validity of its ideas [2].

Aside from the good reasons to study charm particles we already listed above, we have also to mention the possible tests of the Standard Model (SM). Effects like $D^0 - \bar{D}^0$ Mixing, Flavor Changing Neutral Currents (FCNC), Radiative decays and so on, which are allowed only in second order by the SM, have experimental upper limits still very distant from the theoretical predictions. Thus, the charm sector is also a good laboratory to perform searches for effects beyond the Standard Model [3].

Here, we present a basic introduction to the experimental data analysis involving charm decays in fixed target experiments. Although sometimes we present very specific methods, it doesn't mean that they can not be applied for non-charm decays or collider experiments. Since it is an introductory course, we limit ourselves to the study of one of the simpliest and more general kinds of decay, where a charm meson decays into few charged particles, allowing the final state to be totally reconstructed. In the next section, we discuss the method to observe charm particles, from the basic concepts to event selection. Then, we present the fundamental steps of data analysis, first for a high statistical channel and then following to channels with lower statistics. Finally, we present some conclusions.

Observation of Charm Particles

Mean Free Path

The lifetime τ is related to the predominant kind of interaction suffered by the decaying particle. Particles which decay through strong interactions, for example, have small lifetimes ($\sim 10^{-20}s$). For particles decaying through weak interactions, the lifetimes are in general greater and can vary significantly, as can be seen in Table 1.

The lifetime is not Lorentz invariant, thus it depends on the frame where it is measured. By convention, it is defined in the particle rest frame. So, if we say that the pion has a lifetime $\tau = 2.6 \times 10^{-8}s$, we are referring to the lifetime measured in the rest frame of this meson.

The mean free path of a particle in the laboratory is obtained by the product of its velocity v and the lifetime at the laboratory frame, $\tau\gamma$, where $\gamma = E/m$ and E and m are the particle energy and mass, respectively. The mean free path of a particle in the laboratory is, then, given by:

$$< \Delta Z >= c\tau\gamma \ , \tag{2}$$

where c is the light velocity, which is a good approximation for the particle velocity at high energy.

Table 1: Mass, lifetime and mean free path for some known particles.

Particle	$\tau(s)$	Mass(GeV)	$< \Delta Z >$ at 30GeV
$\pi^+(u\bar{d})$	2.6×10^{-8}	0.14	$1.5km$
$K^+(u\bar{s})$	1.24×10^{-8}	0.494	$220m$
$p(uud)$	$> 10^{32}$ yrs	0.938	$> 10^{33}$ light yrs
e^-	$> 10^{22}$ yrs	0.0005	$> 10^{27}$ light yrs
μ^-	2.2×10^{-6}	0.106	$200km$
$\Sigma^-(dds)$	1.5×10^{-10}	1.197	$1m$
$D^+(c\bar{d})$	1.06×10^{-12}	1.869	$0.5cm$
$D^0(c\bar{u})$	4.2×10^{-13}	1.865	$0.2cm$
$D_s^+(c\bar{s})$	4.5×10^{-13}	1.970	$0.2cm$
$\Lambda_c^+(udc)$	2.0×10^{-13}	2.285	$0.1cm$

In Table 1 we list some known particles with their lifetimes, masses, and the mean free path for 30GeV. For a 20 meters long detector, almost all charged particles like pions, kaons, protons, electrons and muons can cross it. Thus, with an appropriate detector, we can get their trajectories, momenta, energy and nature.

Charm particles, however, have smaller lifetime and higher mass, which implies that tipically they can travel distances of the order of centimeters, depending on the energy. That means that in general they cannot be observed directly and thus indirect measurements are needed.

Invariant Mass

Usually, charm particles are observed detecting their decay products. From the conservation of 4-*momentum* and relativistic rest mass invariance, we can associate the decay products with the original particle.

Let us take a simple example of the decay $D^0 \to K^-\pi^+$. As we know, the square of the 4-*momentum* vector is equal to the square of the mass, $P^2 = E^2 - |\vec{P}|^2 = M^2$. By 4-*momentum* conservation we have:

$$M_D^2 = (P_K^\mu + P_\pi^\mu)^2 = P_K^2 + P_\pi^2 + 2P_K^\mu P_{\pi\mu} \ . \tag{3}$$

Thus,

$$M_D^2 = m_K^2 + m_\pi^2 + 2(\vec{P}_K^2 + m_K^2)^{1/2}(\vec{P}_\pi^2 + m_\pi^2)^{1/2} - 2\vec{P}_K.\vec{P}_\pi \ . \tag{4}$$

From this equation, we see the necessary information that a detector must give to perform a spectroscopy analysis: i) the *momentum* vectors of the produced particles; ii) nature of these particles, to correctly assign their masses in the above equation.

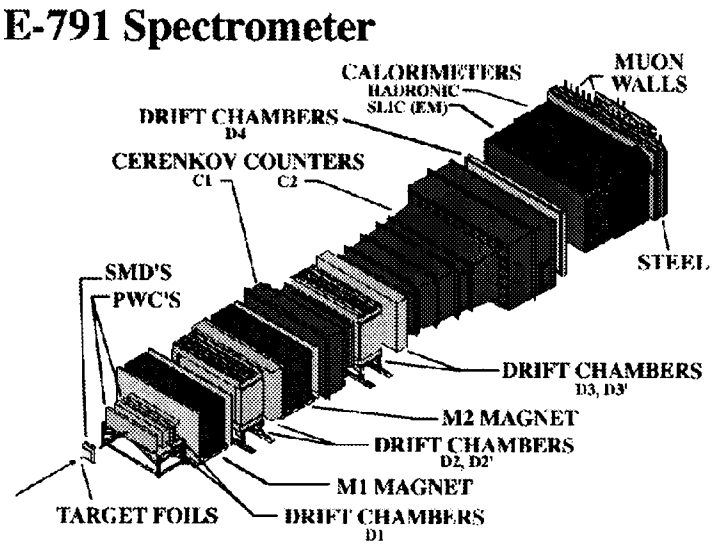

Figure 1: The E-791 Spectrometer.

Detectors

Let us take as an example the detector used by E-791, a fixed target hadroproduction experiment at Fermilab. The detector is shown in figure 1. To determine the *momentum* vector of the particles, Silicon Microstrip Detectors (SMD), drift-chambers and magnets are used. To determine the nature of the particles, calorimeters, Čerenkov counters and muon counters are used. We briefly describe these detectors below.

Tracking System and Momentum Determination

At the front end of the spectrometer, just after the target foils, there is a set of SMD's, solid-state detectors with excellent spacial resolution ($\sim 10^{-3} cm$). They constitute the first information for the tracking system and, because of the good resolution, they can separate very well the point where the charm particle is produced and the point where it decays. This information is crucial for charm analysis in fixed target experiments.

The spectrometer has four stations of drift-chambers used to complete the tracking information. They are made with a ionizing gas and negatively charged wires. When a charged particle crosses the detector, it can ionize the gas and the free electrons produced then drift creating an avalanche of electrons near the collecting wire. Each station has a set of drift-chambers with the wire planes oriented in different directions, in order to have all the coordinates of the particle with a resolution of about $1mm$.

Two magnets, one between the first and second drift-chamber stations and the other between the second and third ones, are used to deflect the particle

trajectories. The angle of deflection dependes on the momentum by:

$$\theta \cong \frac{\int^L B(l)\, dl}{3.33p}\,, \tag{5}$$

where B is the magnetic filed, p is the *momentum* of the particle, l is the position along the trajectory in the magnet and L is the length of the magnet. Thus, from the deflection angle θ the *momentum* of the charged particle is obtained.

Particle Identification

Čerenkov counters and calorimeters are widely used in particle physics to identify particles. The E-791 experiment has 2 Čerenkov detectors, hadronic and electromagnetic calorimeters. At the back end of the spectrometer, there are also scintillators to detect muons.

The Čerenkov detectors can give information on the particle nature based on the fact that a particle with velocity greater than the light velocity in a given medium emits photons. The number of emited photons depends on the *momentum* and mass of the particle [1]. A Čerenkov counter is constituted of a gas path where the Čerenkov light is produced and spherical mirrors aimed at photomultipliers which focus and count the photons, respectively.

The electromagnetic calorimeter is composed of a series of lead foils interlaced with liquid scintillator. The lead foils act as radiators, electrons deposite their energy by *Bremsstrahlung* and photons by pair creation, producing a cascade mechanism, which can be detected by the scintillator.

The hadronic calorimeter is made with steel and plastic scintillators, with structure very similar to the electromagnetic calorimeter, and located just after it. Hadrons deposit their energy by hadronic interactions. This detector is particularly useful to identify neutral particles, which are invisible for the most part of the spectrometer.

After the hadronic calorimeter, there is a steel absorber wall to prevent any other particles but muons to arrive at the scintillators located behind it. So, detecting a particle by one of these scintillators is a positive indication of the presence of a muon.

Event Selection

From hadron-nucleon inelastic interactions, just one in 10^3 events has charm particles. So, critera to select charm candidate events are needed. A typical charm event has the following features:

- The $c - \bar{c}$ pairs are produced with higher tranverse *momentum* relative to lighter quarks. Thus, a first selection made by E-791 is to ask for events with high "transverse energy" (E_T), that is, from the data of the calorimeters, a weighted sum of the deposited energies is made favoring signals more distant from the beam line.

[1] For a more detailed discussion on this subject, see reference [4].

- It has a clear interacting point, called primary vertex. The primary vertex is determined by the point where a number of charged tracks converge inside the target.

- It has one (or two) secondary vertices, that is, probably points of charm particle decays.

A very illustrative example of a charm event production is shown in figure 2. This event is from E-687, a fixed target photo-production experiment at Fermilab. We can clearly see the primary vertex - the first point at the left (formed by tracks 1, 3, 8, 10 and 11) and then two secondary vertices. The first one (formed by tracks 2 and 6) is a good $D^0 \to K^-\pi^+$ candidate, while the second (formed by tracks 4, 5, 7 and 12) is a $\bar{D}^0 \to K^+\pi^+\pi^-\pi^-$ candidate.

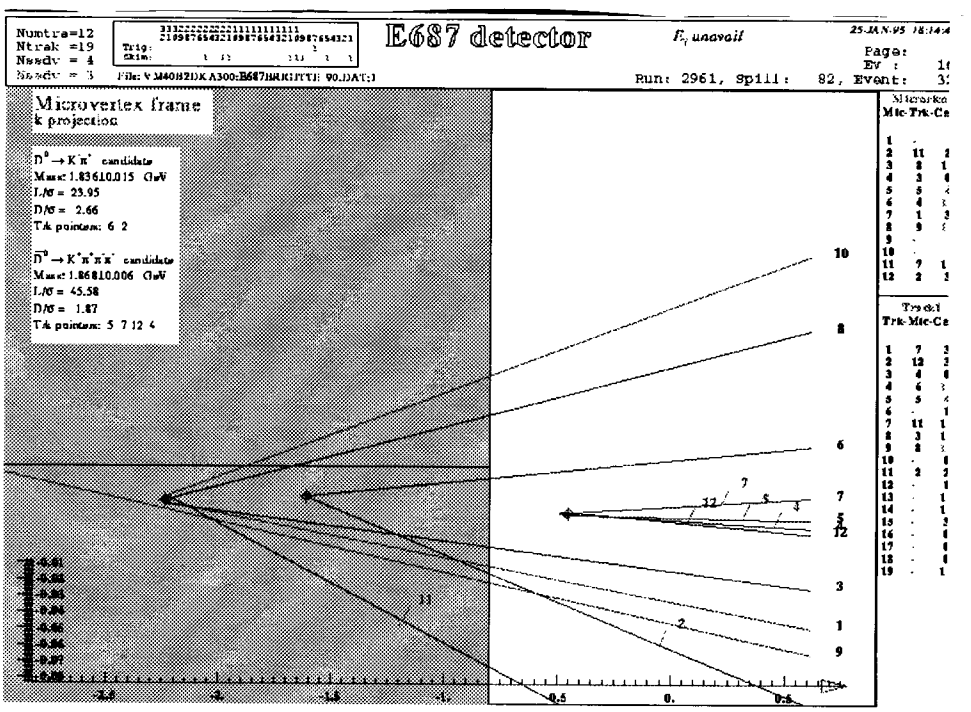

Figure 2: Double Charm Event in Experiment E-687.

In general, a charm decay has the primary and secondary vertices well separated. Thus, another selection can be made using this feature. In E-791, a first selection of this kind was made during data reconstruction; for example, for secondary vertices formed by three charged tracks it was required that:

$$Z_{sec} - Z_{pri} > 4\sqrt{\sigma_{pri}^2 + \sigma_{sec}^2}\ , \tag{6}$$

where Z_{sec} and Z_{pri} are the z coordinates of secondary and primary vertices respectively and σ_{pri} and σ_{sec} are the associated errors. This first selection

could reduced the original E-791 sample of 20 billion recorded events to 2 billion.

DATA ANALYSIS

After the general charm decay selection, based on event tranverse energy and separation of primary and secondary vertices, new selections based now on specific decay modes are required. For example, when performing an $D^0 \to K^-\pi^+$ analysis, it is necessary to ask, among other things, for a secondary vertex formed by two and only two charged tracks, one compatible with a kaon candidate and the other a pion candidate.

Here, we are going to exemplify an analysis process using three body charm decays. We begin with a high statistics decay mode, $D^+ \to K^-\pi^+\pi^+$, and then follow with medium and low statistics decay modes.

The $D^+ \to K^-\pi^+\pi^+$ Analysis

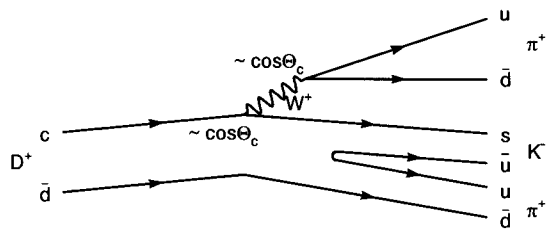

Figure 3: First order diagram of $D^+ \to K^-\pi^+\pi^+$ decay.

The $D^+ \to K^-\pi^+\pi^+$ is the most abundant D^+ channel decaying to three charged particles. In first order, it is represented by the diagram in figure 3. As we can see, both weak vertices are Cabibbo favored, that is, the amplitudes are proportional to the cosine of the Cabibbo angle. Its branching ratio is [5]:

$$BR(D^+ \to K^-\pi^+\pi^+) = (9.1 \pm 0.6)\% \ . \tag{7}$$

To select possible $D^+ \to K^-\pi^+\pi^+$ decays, we begin asking for events with:

- Secondary vertex with three charged tracks.
- Absolute sum of the three charges equal to one.
- Invariant Mass from 1.75 to 2.0 GeV, since D^+ mass is 1.869 GeV. Here, the mass is evaluated associating the opposite charge track to kaon and the other two to pions.
- $Z_{sec} - Z_{pri} > 8\sqrt{\sigma_{pri}^2 + \sigma_{sec}^2}$.

For each $D^+ \to K^-\pi^+\pi^+$ candidate event passed by these criteria, the invariant mass found is plotted. In figure 4, we show this spectrum for about 15% of E-791 data sample, using bins of 10 MeV. We can see that in the D^+ mass region between 1.84 and 1.89 GeV there is a big enhancement in the number of events. This peak represents the $D^+ \to K^-\pi^+\pi^+$ signal, while the remaining events are background.

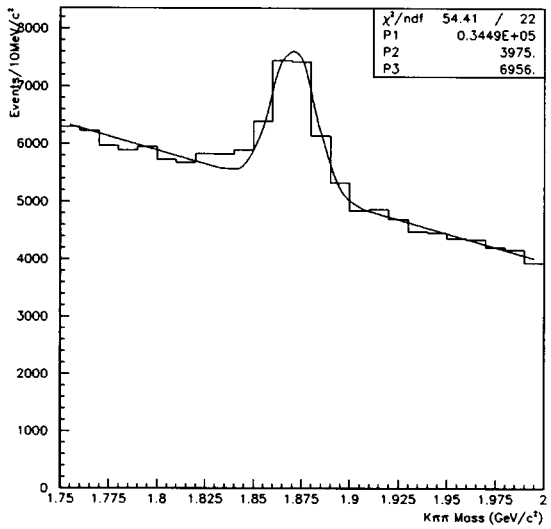

Figure 4: $D^+ \to K^-\pi^+\pi^+$ signal with 15% of E-791 data.

In order to quantify the number of $D^+ \to K^-\pi^+\pi^+$ events, it is necessary to fit the obtained spectrum to a function, which has to take into account the signal and background contributions. In this case, we can fit the signal to a gaussian distribution and the background to a linear function. The gaussian distribution is given by:

$$F(M, N, M_D, \sigma) = \frac{N}{\sqrt{2\pi}\sigma} \exp \frac{(M - M_D)^2}{2\sigma^2} , \tag{8}$$

where M_D, the mass of D^+, is the mean value of the gaussian, σ is the width, related to the *momentum* and angle resolution of the detector, and N is the number of events in the distribution, since the gaussian is normalized to unity.

The fit results (also shown in figure 4) give 6956 ± 182 of $D^+ \to K^-\pi^+\pi^+$ events (value of P3 in the histogram), while under the signal (from 1.84 to 1.9 GeV there are about 34500 (P1) background events. Thus, the signal over background ratio is $S/B = 1/5$.

Thus, the next analysis step is the attempt to reject the background, while mantaining the signal events as much as possible. To do this most effectively, it is necessary to understand the background sources and look for features that can distinguish these events from good $D^+ \to K^-\pi^+\pi^+$ candidates. In the next subsection, we briefly describe the most common types of background in a fixed target experiment like E-791.

Background

In general, we can distinguish between three sources of background: combinatorial background, rescattering and reflections. The last one becomes more important for medium and low statistics channels, so it will be explained later.

The combinatorial background comes from the reconstruction of a fake secondary vertex, that is, three tracks that do not come from a single charm decay can form a vertex accidentally. In general, this happens due to bad track and vertex reconstruction.

The second type of background, rescattering, occurs when a particle produced by the beam-target interaction suffers a new interaction with a nucleon, probably producing new particles. This process can also simulate a secondary vertex.

The combinatorial background and rescattering are in general parametrized by a straight line or an exponential function, since they have a random distribution governed only by phase space limitations.

The Set of Cuts

As we said before, it is necessary to adopt selection criteria - usually called a set of "cuts" - in order to reject as many background events as possible, without loosing too much signal.

In fixed target experiments, in general the cuts can be divided in two classes: identification cuts and vertex/track cuts. The first one uses information on the particle nature and the last is based on the quality of the vertices or tracks.

Vertex Cuts. Let's begin exemplifying useful vertex cuts. The first and maybe the most important of them is related to the distance between primary and secondary vertices, like in equation (6). In fact, we can define a scaled delta Z variable, SDZ, given by:

$$SDZ = \frac{Z_{sec} - Z_{pri}}{\sqrt{\sigma_{pri}^2 + \sigma_{sec}^2}} \,. \tag{9}$$

This variable measures the distance between primary and secondary vertices in terms of the associated errors on these variables. Since both the distance and the errors depend on the *momentum* of the charm particle, the SDZ variable is nearly *momentum* independent. In figure 5 we can see typical SDZ distributions (up to $SDZ = 50$) for $D^+ \to K^-\pi^+\pi^+$ signal events[2] and background (taken outside D^+ mass region). Clearly, background events are concentrated at low SDZ values.

In fact, a cut on $SDZ > 20$, for example, rejects 62% of background, retaining 77% of $D^+ \to K^-\pi^+\pi^+$ signal events. The resulting mass spectrum after this cut is shown in figure 6. Now, the signal/background ratio is about 1/2, that is, 2.5 times bigger than the one with $SDZ > 8$ (figure 4).

[2]In fact, the SDZ distribution shown in figure 5(a) is from simulated Monte Carlo events, as will be discussed later. From here on, when we refer to the signal distribution of a given variable, we will be using Monte Carlo data.

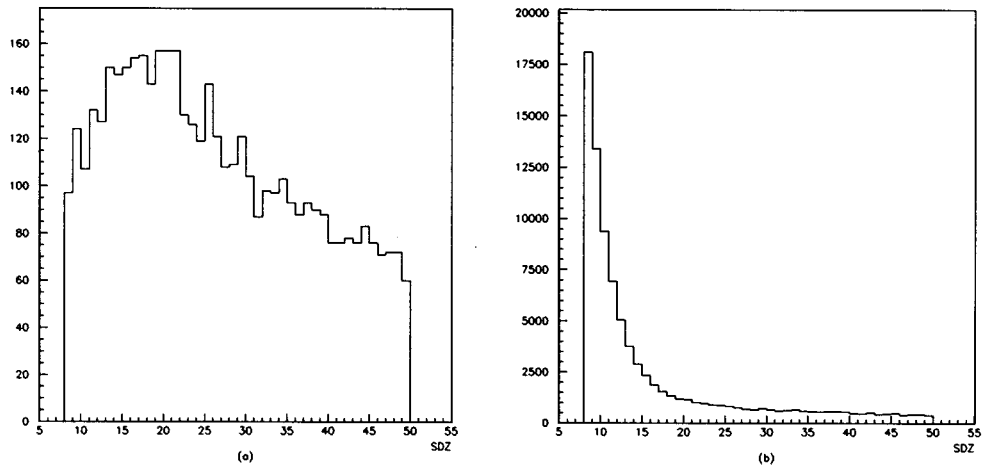

Figure 5: SDZ Distributions for (a) $D^+ \to K^-\pi^+\pi^+$ Signal; (b) Background events.

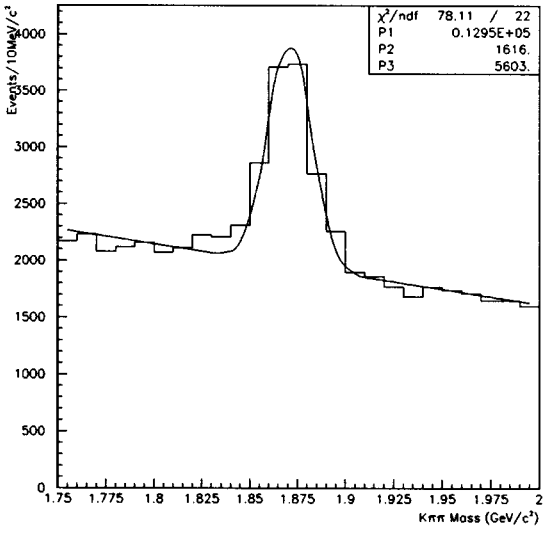

Figure 6: $D^+ \to K^-\pi^+\pi^+$ signal with $SDZ > 20$.

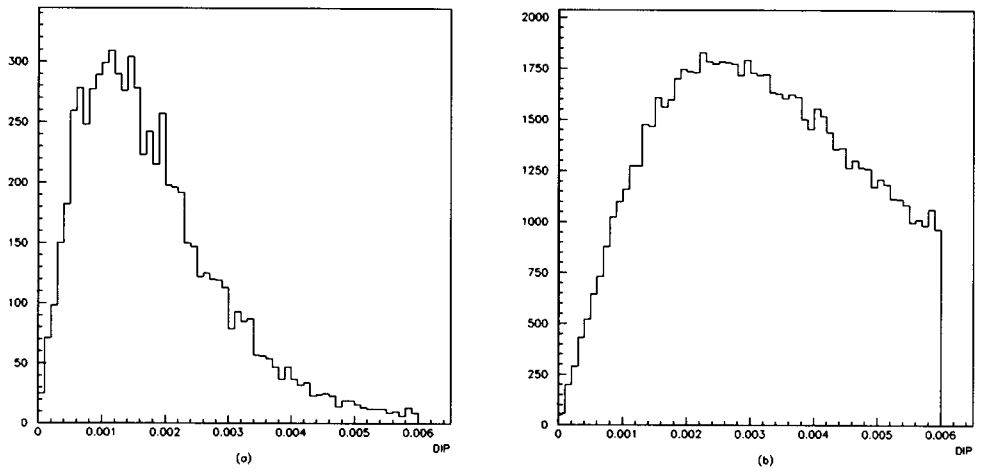

Figure 7: DIP Distribution for(a) $D^+ \rightarrow K^-\pi^+\pi^+$ Signal; (b) Background events.

Another useful variable to discard background is the impact parameter of the reconstructed *momentum* of the charm particle with respect to the primary vertex - DIP. Since the charm particle is produced in the primary vertex, it is expected the DIP variable to be very small for signal events. For the combinatorial background, a random distribution is expected. In figure 7 we shown signal and background distributions for this variable. If we choose to cut on $DIP < 30\mu m$, for example, we retain 84% of the signal and reject 62% of background.

Up to now, the two variables defined are specially useful against combinatorial background. In the case of rescattering, we can make use of the fact that in E-791 the targets were segmented. In figure 8 we show the distribution of the reconstructed primary vertex positions - we can see clearly the different position of each target. Thus, a very good way to avoid events with a secondary interaction faking a decay vertex is eliminating events for which the secondary vertex is located inside one of the targets. The variable SIGMA measures, in units of σ_{sec}, the distance of the secondary vertex from the closest target edge. For $SIGMA < 0$, the secondary vertex is located inside the target. In figure 9 we show the $SIGMA$ distribution for $D^+ \rightarrow K^-\pi^+\pi^+$ signal and background, where the cut $SIGMA > 0$ is already imposed.

Identification Cuts. To distinguish between protons, kaons and pions, two Čerenkov detectors - C1 and C2 - were used in E-791, with different gas mixtures. The expected distribution of the number of photons produced as a function of *momentum* for each of these particles is shown in figure 10 for both counters C1 and C2. If we observe, for example, that a particle with 30 GeV produced photons in C1 but not in C2, it means it is a good kaon candidate. In general, however, the Čerenkov detectors cannot define precisely the particle nature. What they can give us is the probability of a given particle to be a pion, or a proton, etc, depending of the number of photons produced in each Čerenkov detector and the particle *momentum* . Sometimes, actually, they just have no information at all, meaning that the particle was not detected or the information is confused. In these cases, there is associated to this particle

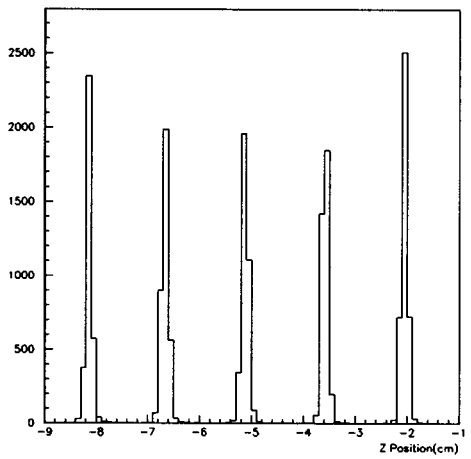

Figure 8: Reconstructed Position of the Primary Vertex for $D^+ \to K^-\pi^+\pi^+$ events.

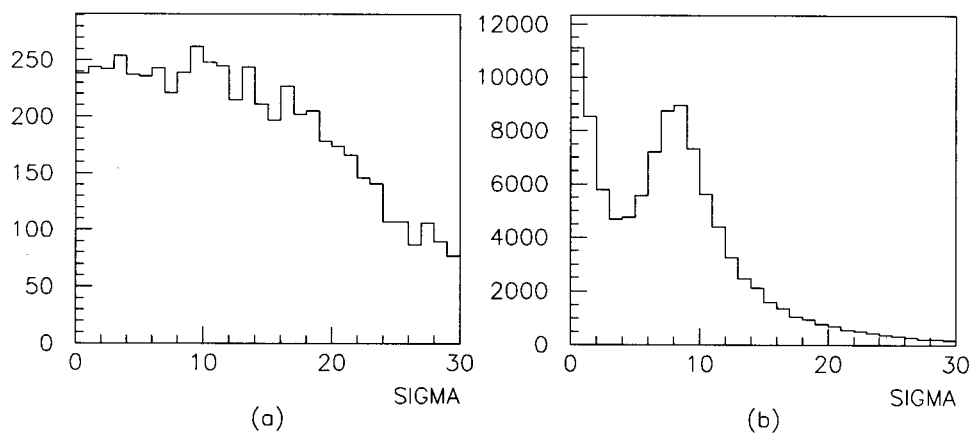

Figure 9: $SIGMA$ Distribution for (a) $D^+ \to K^-\pi^+\pi^+$ Signal; (b) Background events.

the *a priori* probability, related to the percentage of kaons, pions, protons, etc, produced by the experiment. For example, 84% of the hadrons produced are pions, 12% are kaons and 4% are protons; thus, these will be the probabilities the Čerenkov detector software will give when the detectors have no information.

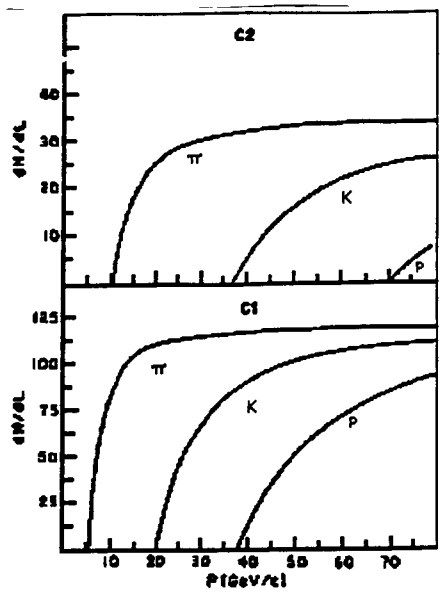

Figure 10: Number of emited photons per unit length of the counters C1 and C2 as a function of *momentum* .

In figure 11(a) we show the kaon probability distribution for the opposite charge track[3] of each $D^+ \to K^-\pi^+\pi^+$ event and the analogous for background in figure 11(b). Both have a peak at 12%, which is the kaon *a priori* probability, but the signal events have also a clear peak at 75%. This peak is the response of the Čerenkov counters when they can affirm that the particle is not a pion, thus it can be a kaon with 75% of probability or a proton with 25%. The peak in zero occurs when the Čerenkov can say that the particle is not a kaon and the peak near 1 is when they can assure the particle is a kaon. For the same events shown in figure 11, there are analogous distributions for pion and proton probabilities.

If we cut, for example, on kaon Čerenkov probability $PK > 0.2$, we eliminate the events with *a priori* probability, representing 84% of background events.

First Results

When we apply our first and intuitive set of cuts $SDZ > 20$, $DIP < 30\mu m$ and Čerenkov identification for kaon track $PK > 0.2$, we obtain the spectrum

[3]Note that the opposite charge track of the decay $D^+ \to K^-\pi^+\pi^+$ is naturally the kaon candidate.

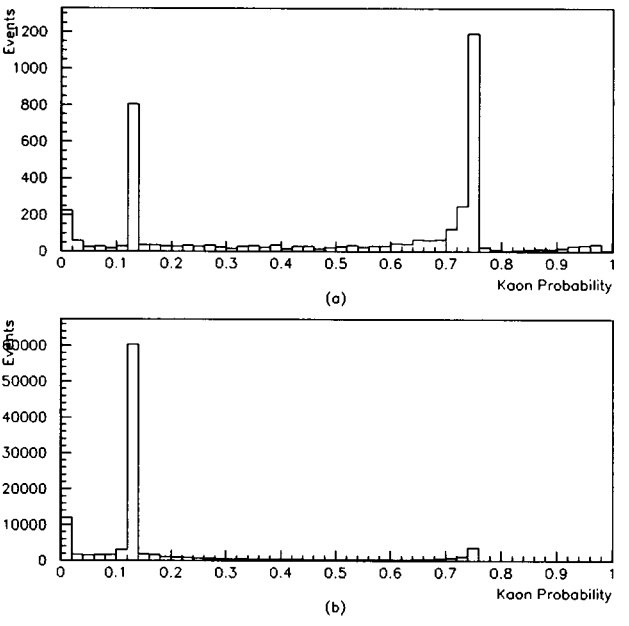

Figure 11: Čerenkov Probability Distribution of the kaon candidate for (a) $D^+ \to K^-\pi^+\pi^+$ Signal; (b) Background events.

shown in figure 12. We can see that the background under the signal drops from the original 34500 events of figure 4 to about 400 events, while the signal falls from 6956 ± 182 to 2513 ± 54. Thus, the signal/background ratio is now $S/B = 6$, 30 times bigger than the one obtained in figure 4.

Statistical Significance

In the previous subsection, we have shown the resulting $D^+ \to K^-\pi^+\pi^+$ spectrum after the application of a set of cuts chosen based on a qualitative comparison between the signal and background. However, to establish a final and trustworthy set of cuts, a less subjective method is required.

As we said before, when we choose a set of cuts, we want to keep the signal events and have the minimum number of background events. The last condition is important for a small statistical error. The main goal is, in fact, try to find a selection criterium that can give the best statistical significance, that is, the best signal/error ratio. The statistical error associated with the number of signal events is given by the possibility of signal and background fluctuation, i.e., it is obtained by the square root of the sum of signal and background (under the signal) events (assuming a poisson distribution). Thus, the best set of cuts is the one which maximizes the relation:

$$Significance = \frac{S}{\sqrt{S+B}}, \tag{10}$$

where S is the number of signal events and B is the number of background events[4].

[4]When $B >> S$, it is also very common to maximize $\frac{S}{\sqrt{B}}$ instead of $\frac{S}{\sqrt{S+B}}$.

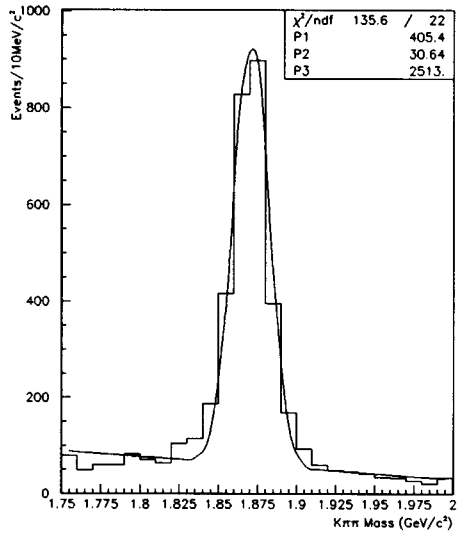

Figure 12: $D^+ \to K^-\pi^+\pi^+$ signal with $SDZ > 20$, $DIP < 30\mu m$ and $PK > 0.2$.

In general, the error on the signal events represents one stardard deviation. This value covers 68% of the signal for a gaussian distribution. Two and three standard deviation cover 95% and 99.7% respectively. These numbers are associated with the probability of fluctuation. Thus, if we have a signal for which the number of events is three times the associated error, or in other words, a signal with statistical significance of three stardard deviations, the probability that this signal is just a background fluctuation is less than 0.3%. By convention, in general a signal has credibility if the statistical significance is greater than three standard deviations.

Thus, the higher the statistical significance of the signal, the higher is the reliability of the results, since the less is the probability of fluctuation. One of the important parts of an analysis is, in fact, to obtain a set of selection criteria with the highest statistical significance.

When analysing a high statistics channel like as $D^+ \to K^-\pi^+\pi^+$, even with loose cuts it is clearly possible to distinguish between signal and background and the possible fluctuations on the number of events in the signal are small. In this case, it is possible to determine the best set of cuts from the number of events in the signal and background, maximizing the significance using equation (10).

However, for medium or low statistics channels, the number of events in the signal is smaller. The background level can be much higher than the signal and can even impede its observation. Nowadays, for example, the number of events for singly and doubly Cabibbo supressed decays can vary from 10 to 10^3.

In these cases, it is very difficult to perform an optimization of the cuts using the number of events in the actual signal, since possible fluctuations can change significantly the results, sometimes incorrectly favoring a given set of cuts. Thus, another optmization criterion is necessary for medium and low

statistics channels.

Monte Carlo

To solve the question raised in the previous section, a very important tool, widely used in high energy physics, is the simulation of signal events. The main goal is to reproduce by computation the interaction between beam and target producing new particles, as in real data events. In particular, we can generate events containing a specific charm particle decaying in a given decay mode. We can generate as many events as we wish, independent of whether the decay mode is favored or highly supressed.

Simulated events are created by a generator of random numbers which uses all the knowledge we have about production (Lund Model) and decay properties of the known particles, and also relativistic kinematics, which is very important for the behavior of the particles inside the detector. These events are called Monte Carlo events. After generation, the next stage is the simulation the detector, that is, the simulation of all detector responses to the produced particles. This stage is called digitization, and it has to reproduce all the details of the each detector, including the inefficiencies and electronic noise.

After generation and digitization, Monte Carlo events are as equal as possible to real events. As we said before, since they are simulated events, we can choose the decay modes we want to have in a particular Monte Carlo sample and also the quantity. For example, we can produce 50,000 events demanding that each event produce a D^+ and that all D^+ decay into $K^-\pi^+\pi^+$. Due to this feature, Monte Carlo (MC) samples are almost free from background.

In figure 13 we show the spectrum of a MC sample of the decay $D^+ \rightarrow K^-\pi^+\pi^+$, using the same cuts used for data events (fig.12). We can see that the background level is below 10 events per bin, completely different from the spectrum of figure 12. In fact, here the S/B ratio is about 65.

With a clean sample like this, reproducing all the features of a real event, it is possible to:

- Study the behavior of particular channels, without background, whether they are Cabibbo supressed, Cabibbo allowed or even forbidden decays. In particular, we can study the distribution of the analysis variables for a given decay mode, as we did before using the $D^+ \rightarrow K^-\pi^+\pi^+$ channel.

- Find the efficiency of each of the cuts on the variables and the global efficiency for a given set of cuts. For example, if we produce 100,000 $D^+ \rightarrow K^-\pi^+\pi^+$ MC events and, after applying the set of cuts $SDZ > 20$, $PK > 0.2$, $DIP < 30\mu m$ there are 2000 left, we know that the global efficiency, including geometrical acceptance and reconstruction efficiency, is 2%.

- Optimization of the cuts for medium and low statistical channels. In these cases, to maximize the statistical significance, we substitute the

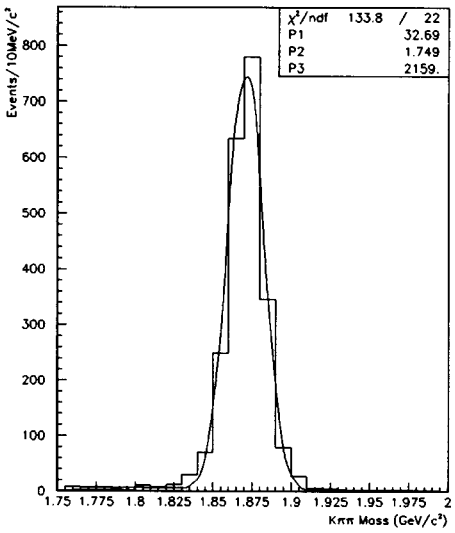

Figure 13: $D^+ \to K^-\pi^+\pi^+$ Monte Carlo signal with $SDZ > 20$, $DIP < 30\mu m$ and $PK > 0.2$.

number signal events in the numerator of equation (10) by the number of MC events:

$$Significance = \frac{S_{MC}}{\sqrt{S+B}}. \tag{11}$$

Note that using the number of MC events is equivalent to using the number of real events since they shall have, in principle, the same position for the maximum of the significance, with the advantage of the first being numerically bigger. In the denominator, however, we still use the number of signal events, since the relation is not linear. It is associated with the expected error and, thus depends fundamentaly on the statistics of the real data sample.

The last item above is particularly important and Monte Carlo simulation can really be very advantageous. In fact, we have a sample free from statistical fluctuations, since we can generate an arbitrary number of events - S_{MC} is as big as we desire. We also have, in this way, an independent sample.

Cuts Optimization

In this section, we are going to perform, in a simplified way, the optimization of the cuts SDZ, DIP, PK and $SIGMA$ for the $D^+ \to K^-\pi^+\pi^+$ analysis. That is, we'll search for the values of these variables which produce the best statistical significance, maximizing the significance in equation (11). For $D^+ \to K^-\pi^+\pi^+$ analysis which has high statistics, as we said before, it is not necessary to use MC to optimize the cuts, but here we are going to use it to illustrate the method.

We begin with loose cuts, $SDZ > 8$, $DIP < 60\mu m$, $PK > 0$ and $SIGMA > 0$. We obtain the number of MC signal events, S_{MC}, and the total number of data events from 1.85 and 1.89 GeV (this will give $S+B$). Thus, we obtain the

statistical significance for this first choice of cuts. Then, we begin to vary the SDZ variable, for example, keeping the other ones fixed at the original value. For each SDZ value, we obtain the statistical significance by equation (11). The resulting curve is shown in figure 14(a). We repeat this process for the three other variables, DIP, PK and $SIGMA$ and obtain the curves shown in figures 14(b), 14(c) and 14(d), respectively.

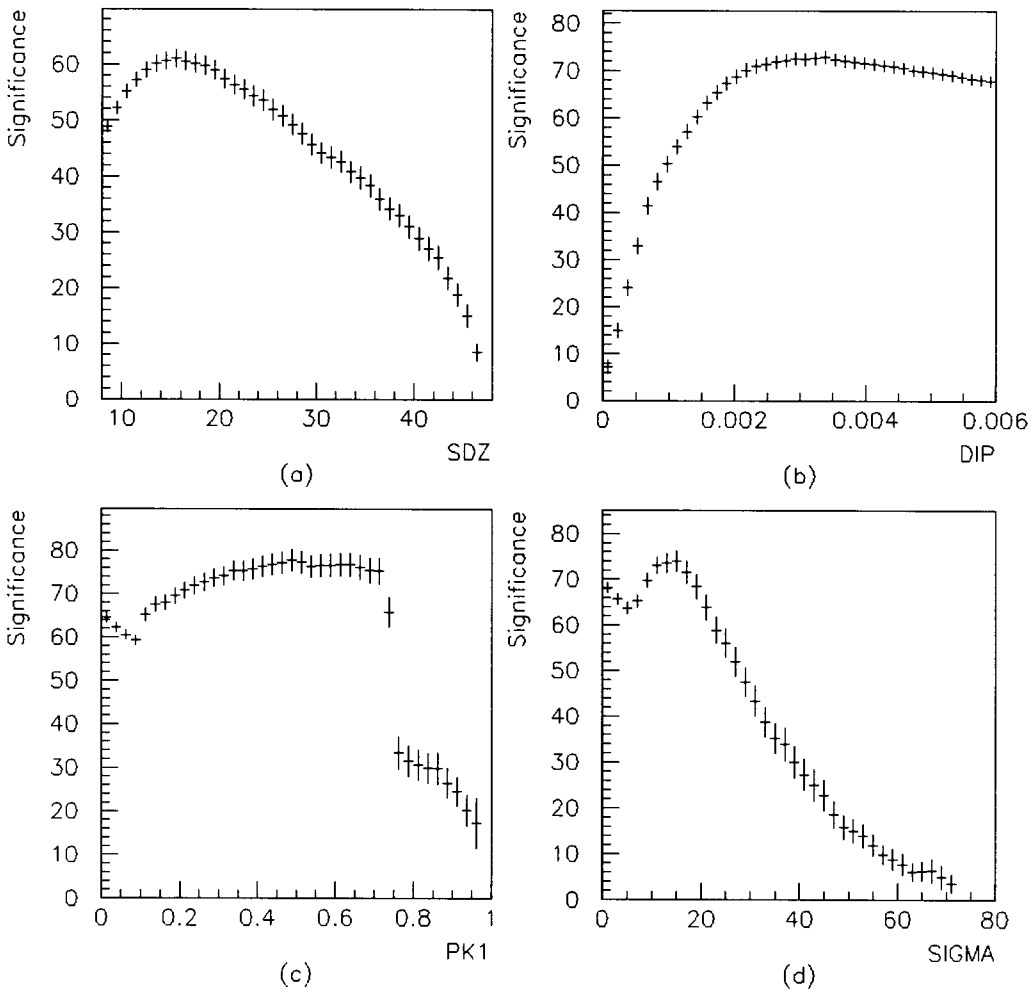

Figure 14: Statistical Significance distribution for (a) SDZ; (b) DIP; (c) PK; (d) SIGMA.

From the results, we got the best values as $SDZ > 15$, $DIP < 30\mu m$ and $PK > 0.5$ and $SIGMA > 15$. However, if we begin this process again with one of the variables, but now fixing the others by the optimized values, we get a different value, showing that we can not optimize the variables independently. In fact, we show in figure 15 the new distribution for $SIGMA$, taking $SDZ > 15$, $DIP < 30\mu m$ and $PK > 0.5$. Now, the optimum value is $SIGMA > 0$ instead of $SIGMA > 15$.

To find the best set of cuts, an iterative process of optimization is thus required. We begin with a given and reazonable set of cuts, maximize the

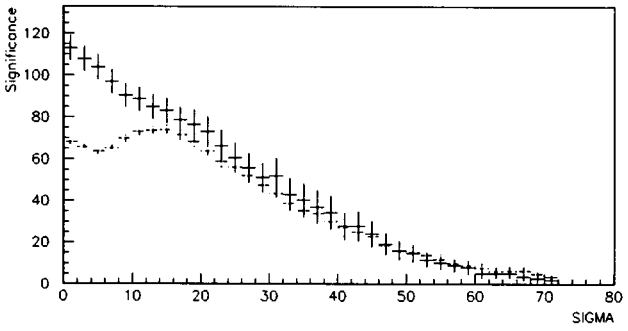

Figure 15: Statistical Significance distribution for $SIGMA$. The dashed points are the same shown before and the solid points were get with the first optimization results for the other variables.

significance for each of the cuts, then repeat the process with the new values until a stability for the cuts is achieved. At this point, the final set of cuts gives the best statistical significance for the signal.

Optimization Results

After performing the optimization process described in the previous section for the $D^+ \to K^-\pi^+\pi^+$ signal, we got the following values: $SDZ > 14$, $DIP < 35\mu m$, $PK > 0.3$ and $SIGMA > 2$. The resulting spectrum for data events is shown in figure 16(a). We obtained 2810 ± 58 $D^+ \to K^-\pi^+\pi^+$ events, corresponding to an statistical significance of 48 stardard deviations.

Using the same set of cuts for a $D^+ \to K^-\pi^+\pi^+$ Monte Carlo sample, we found 2116 ± 47 events for the signal. Since originally 100,000 events were produced, the overall efficiency for this set of cuts is 2.1%. From this number, we obtain the number of $D^+ \to K^-\pi^+\pi^+$ data events produced for 15% of E-791 data: about 140,000.

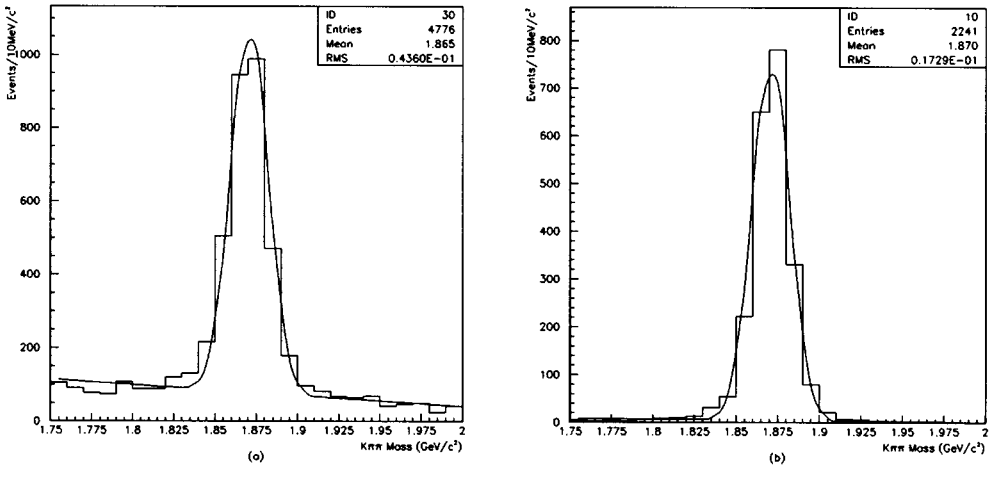

Figure 16: $D^+ \to K^-\pi^+\pi^+$ signal with $SDZ > 14$, $DIP < 35\mu m$, $PK > 0.15$ and $SIGMA > 2$.

Reflections

Up to now, we have been analysing the $D^+ \to K^-\pi^+\pi^+$ channel, which is the most abundant three body decay mode of the meson D^+. As we said before, this channel is Cabibbo favored, the two couplings with the W boson are proportional to the cosine of the Cabibbo angle.

Now, we'll begin to see how an analysis can change when treating channels with lower statistics. In this case, the number of signal events is much smaller and the combinatorial background level can make the observation of the channel difficult. Besides, other charm decay modes, different from the one we want to analyse, can interfere with the results - we call this effect the "reflection" of one channel in the spectrum of another one of interest. This is a very important source of background, as we're going to see below.

The Singly Cabibbo Supressed Decay $D^+ \to \pi^-\pi^+\pi^+$

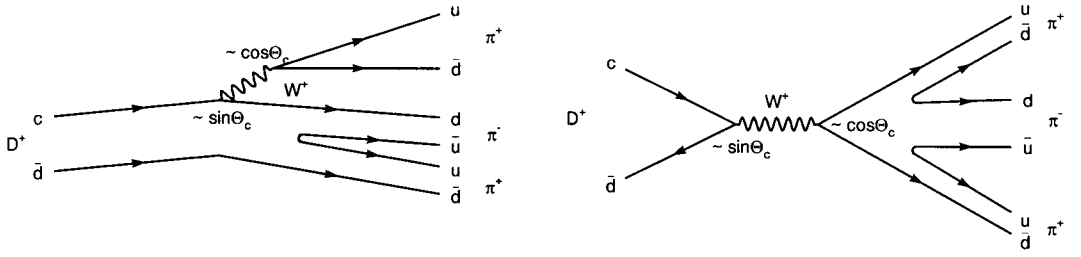

Figure 17: First order diagrams of $D^+ \to \pi^-\pi^+\pi^+$ decay.

The decay mode $D^+ \to \pi^-\pi^+\pi^+$ is singly Cabibbo supressed, that is, the amplitude is proportional to $sin\theta_c$ as can be seen in figure 17. In a qualitative approach, the ratio between the branching ratio of this channel and $D^+ \to K^-\pi^+\pi^+$ may be naively expected to be of the order of the ratio $sin^2\theta_c/cos^2\theta_c \sim 1/20$. In fact, the measured $D^+ \to \pi^-\pi^+\pi^+$ BR is $(3.2 \pm 0.6) \times 10^{-3}$ or 30 times smaller than $D^+ \to K^-\pi^+\pi^+$ BR, a little lower than the above value. If we don't take into account the experimental efficiency difference for these two channels, we can say that the $D^+ \to \pi^-\pi^+\pi^+$ signal will be about 30 times smaller than $D^+ \to K^-\pi^+\pi^+$ signal.

Since the Čerenkov detectors are not perfect, it is possible that they misidentify a kaon as a pion. Let's imagine that, for a given value of the Čerenkov probability, the possibility of misidentifying a kaon as a pion is about 10%. In this case, for each real $D^+ \to \pi^-\pi^+\pi^+$ decay, there will be three events of $D^+ \to K^-\pi^+\pi^+$ where the kaon was identified as pion. These events will appear in the $\pi^-\pi^+\pi^+$ spectrum.

But, for $D^+ \to K^-\pi^+\pi^+$, since the faked pion is actually a kaon, we would be attributing the mass of a pion to a kaon, as can be seen in the expression

for the $\pi^-\pi^+\pi^+$ invariant mass:

$$\begin{aligned} M_D^2 &= m_\pi^2 + 2m_\pi^2 + 2(P_\pi^2 + m_\pi^2)^{1/2}(P_{\pi 1}^2 + m_\pi^2)^{1/2} + \\ & 2(P_\pi^2 + m_\pi^2)^{1/2}(P_{\pi 2}^2 + m_\pi^2)^{1/2} + 2(P_{\pi 1}^2 + m_\pi^2)^{1/2}(P_{\pi 2}^2 + m_\pi^2)^{1/2} - \\ & 2\vec{P}_\pi.\vec{P}_{\pi 1} - 2\vec{P}_K.\vec{P}_{\pi 2} - 2\vec{P}_{\pi 2}.\vec{P}_{\pi 1} \ . \end{aligned} \tag{12}$$

This change will produce a shift of the $D^+ \to K^-\pi^+\pi^+$ events - they will not be centered around D^+ mass anymore, but will be reflected in the $\pi^-\pi^+\pi^+$ spectrum below the D^+ mass, since the pion mass is less than the kaon mass. In figure 18 we show the $\pi^-\pi^+\pi^+$ spectrum[5]. We clearly see the $D^+ \to \pi^-\pi^+\pi^+$ signal centered at the D^+ mass; there is also the Cabibbo favored decay $D_s^+ \to \pi^-\pi^+\pi^+$ around 1.97 GeV, which is the D_s^+ mass, and we see near 1.75 GeV a broad peak, which comes from $D^+ \to K^-\pi^+\pi^+$ decays.

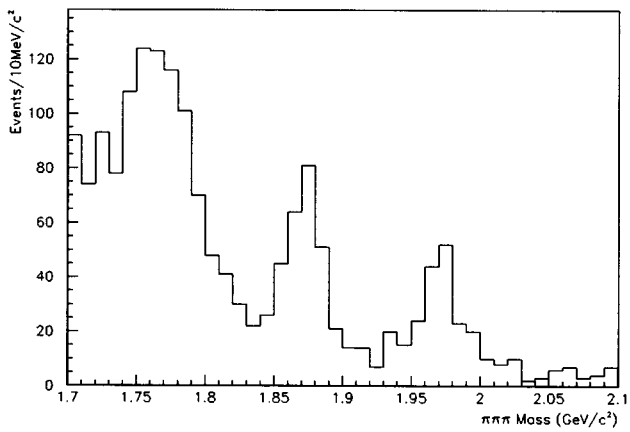

Figure 18: $\pi^-\pi^+\pi^+$ Mass spectrum.

To extract quantitative information from the $\pi^-\pi^+\pi^+$ spectrum, like the numbers of $D^+ \to \pi^-\pi^+\pi^+$ and $D_s^+ \to \pi^-\pi^+\pi^+$ events, we have to fit the data to a sum of functions. Thus, we have to parametrize also the $D^+ \to K^-\pi^+\pi^+$ reflection. To do this, we need two kinds of informations: the position and shape of the reflection and the expected number of reflected events.

The position of the reflection we can get from Monte Carlo, since it is a clean sample. The $D^+ \to K^-\pi^+\pi^+$ events are projected in the $\pi^-\pi^+\pi^+$ spectrum, that is, we atribute to the kaon candidate the pion mass. The resulting spectrum is shown in figure 19(a). To fit the distribution, we used a modified gaussian:

$$F(x, n, \bar{x}, \sigma) = Nk \exp \frac{-\beta^2(x) \times (x - \bar{x})^2}{2\sigma^2} \ ,$$

$$\beta(x) = e^{\lambda(x-\bar{x})} \ . \tag{13}$$

[5]This spectrum was obtained with an optimized set of cuts for this case, with other variables which were not introduced before. The statistics is also different from the one we were presenting for $D^+ \to K^-\pi^+\pi^+$ - now we have about 40% of E-791 data sample.

which has four parameters: the number of events N, the mass central value $\bar{x}$, the width σ and the parameter λ, which provides the assymetric shape for the reflection. The constant k normalizes the modified gaussian to unity. The last three parameters, after the fit, fix the shape and position of the reflection.

The second kind of information, the number of reflected events, is obtained from real data by simply projecting the events in $K^-\pi^+\pi^+$ spectrum and fitting the $D^+ \to K^-\pi^+\pi^+$ signal, as can be seen in figure 19(b). In this way, we get N.

Now, we have the four parameters which characterize the $D^+ \to K^-\pi^+\pi^+$ reflection. To fit the $\pi^-\pi^+\pi^+$ histogram, we fix these parameters and also add two gaussians for the contributions of the signals $D^+ \to \pi^-\pi^+\pi^+$ and $D_s^+ \to \pi^-\pi^+\pi^+$ and an exponential for the smooth background. The resulting spectrum with the total fit function is shown in figure 20. From the fit results, we got 190 ± 18 events for the decay $D^+ \to \pi^-\pi^+\pi^+$ and 132 ± 15 events of $D_s^+ \to \pi^-\pi^+\pi^+$.

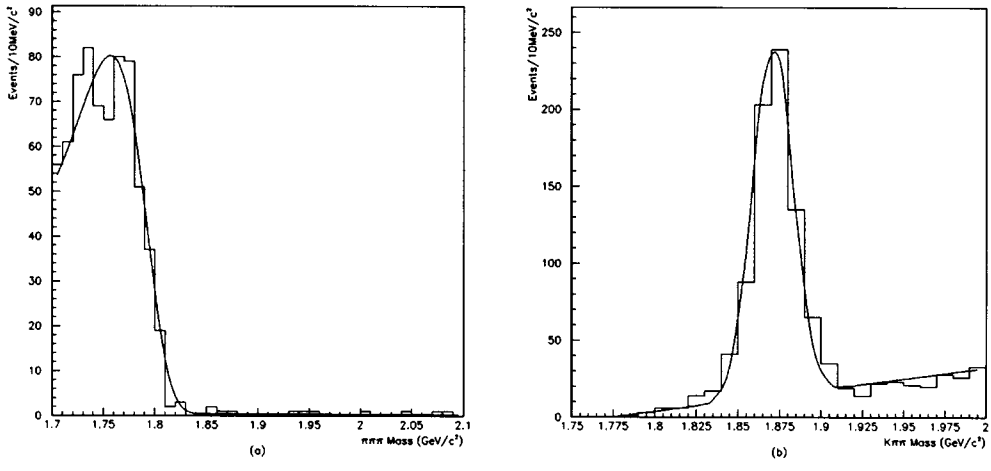

Figure 19: (a) $\pi^-\pi^+\pi^+$ Spectrum for MC $D^+ \to K^-\pi^+\pi^+$ events ; (b) $D^+ \to K^-\pi^+\pi^+$ Events cointained in $\pi\pi\pi$ spectrum.

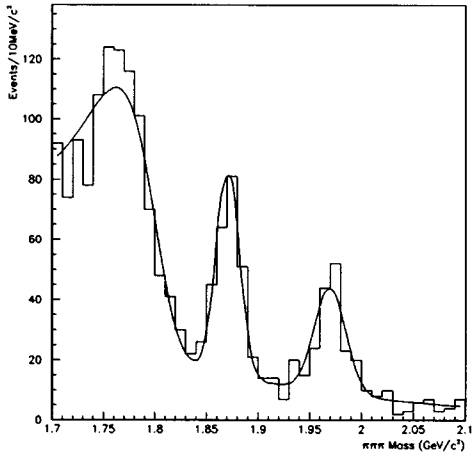

Figure 20: $\pi^-\pi^+\pi^+$ Spectrum with the fit function.

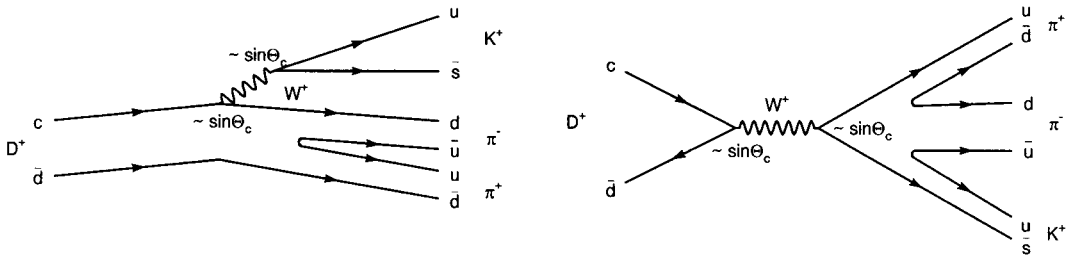

Figure 21: First order diagrams of $D^+ \to K^+\pi^+\pi^-$ decay.

The Doubly Cabibbo Supressed Decay $D^+ \to K^+\pi^+\pi^-$

In general, the smaller the branching ratio of the channel, the larger is the number of expected reflections on its spectrum and thus more complex is the analysis involved. This is precisely what happens for the decay $D^+ \to K^+\pi^+\pi^-$, with double Cabibbo supression, which were recently observed [6, 7]. The two couplings with the W boson have amplitudes proportional to the sine of the Cabibbo angle, as can be seen in figure 21.

In the study performed using E-791 data [7], the most important reflections detected in $K^+\pi^+\pi^-$ spectrum were four three body channels, two of them Singly Cabibbo Supressed decays of D^+:

- $D^+ \to K^-\pi^+\pi^+$
- $D^+ \to K^-K^+\pi^+$
- $D^+ \to \pi^-\pi^+\pi^+$
- $D_s^+ \to K^-K^+\pi^+$

In figure 22(a) we show the contributions of each of these reflections (position, shape and number of events) in the $K^+\pi^+\pi^-$ spectrum with the full E971 data sample. We can clearly see that there are two other peaks in this spectrum: one around 1.87 GeV, which corresponds to the $D^+ \to K^+\pi^+\pi^-$ decay and the other around 1.97 GeV, corresponding to the singly Cabibbo supressed decay $D_s^+ \to K^+\pi^+\pi^-$. In figure 22(b) we show the same spectrum with the final fit function, which is the sum of the above contributions with two gaussians functions for D^+ and D_s^+ signals.

CONCLUSIONS

In this course, we presented in an introductory way the main elements of an analysis of experimental data for the observation of charm particle decays in fixed target experiments. As we said in the Introduction, the method used here is quite general, many of the concepts can be applied for collider experiments or non-charm decays. In fact, except for specific topics like the detector and the variables used to select the events, the other concepts discussed like invariant mass, background, statistical significance, Monte Carlo, efficiency, cuts optimization and reflections are used by different experiments and in any kind of accelerator and detector.

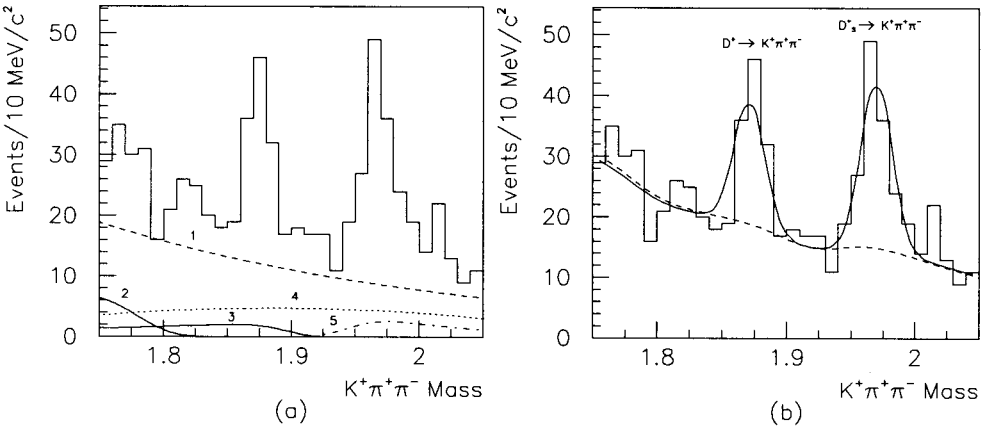

Figure 22: (a) $K^+\pi^+\pi^-$ Spectrum with the following contributions: 1- Background, 2- $D^+ \to K^-K^+\pi^+$, 3- $D_s^+ \to K^-K^+\pi^+$, 4- $D^+ \to K^-\pi^+\pi^+$, 5- $D^+ \to \pi^-\pi^+\pi^+$; (b) $K^+\pi^+\pi^-$ Spectrum with the final fit function.

However, there is a number of different techniques which were not discussed here. To present all of them would be an impossible task, because in high energy physics each experiment and each observation has its own particularities. In fact, in general an experimental research can bring not only a new physical measurement or a better statistical significance of the result but also the originality of the method employed on the observation. This can be done in many distint ways, introducing new cuts, defining new variables, creating new constraints, etc. The important point here is that, to begin an analysis, it is necessary to know the physics involved, how does the detector work, and all possible knowlegde about similar analysis made in other experiments.

It is important to stress that even the subjects presented here were not exhaustely discussed. For those who want to have more information on data analysis on High Energy Physics, we recomend books like the ones listed in reference [8].

ACKNOWLEDGMENTS

We want to thank Jeff Appel and Alberto Reis for useful sugestions and the E791 Collaboration for the use of the data.

References

[1] Gaillard, M.K., Lee, B.W. and Rosner, J.L., *Rev.Mod.Phys.* **47**, 277 (1975); Ellis, J., Gaillard, M.K. and Nanopoulos, D.V., *Nucl.Phys.* **B100**,

313 (1975); Fakirov, D. and Stech, B., *Nucl.Phys.* **B133**, 315 (1978); Cabibbo, N. and Maiani, L., *Phys.Lett.* **73B**, 418 (1978); Cabibbo, N. and Maiani, L., *Phys.Lett.* **79B**, 109 (1978).

[2] Buccella, F. *et al.*, *Phys.Rev.* **51D**, 3978 (1995).

[3] Pakvasa, S., "Charm as a Probe of New Physics", in *Proceedings of CHARM2000 Workshop*, FERMILAB-CONF-94/190.

[4] Fernow, R., *Introduction to Experimental Particle Physics*, Cambridge: Cambridge University Press, 1986.

[5] Particle Data Group, *Phys.Rev.* **D50**, 1173 (1994).

[6] E687 Collaboration, Frabetti, P.L. *et al.*, *Phys.Lett* **B359**, 403 (1995).

[7] Reis, A., representing E791 Collaboration, "Observation of The Doubly Cabibbo Supressed Decay $D^+ \to K^+\pi^+\pi^-$", presented in the Conference *Production and Decay of Hyperons, Charm and Beauty Hadrons*, Strasbourg (1995).

[8] Bock, R.K., Grote, H., Notz, D. and Regler, M., *Data Analysis Techniques for High-Energy Physics Experiments*, Cambridge: Cambridge University Press, 1990; Ferbel, T., *Experimental Techniques In High Energy Physics*, Frontiers in Physics, Massachusets: Addison-Wesley Publishing Company, Inc., 1987; Lyons, L., *Statistics for Nuclear and Particle Physicists*, Cambridge: Cambridge University Press, 1986.